Available online at www.sciencedirect.com
ScienceDirect
Polymer 49 (2008) 254–262
polymer
www.elsevier.com/locate/polymer

Phase separation and dewetting in polystyrene/poly(vinyl methyl ether) blend thin films in a wide thickness range

Hiroki Ogawa, Toshiji Kanaya*, Koji Nishida, Go Matsuba

Institute for Chemical Research, Kyoto University, Uji, Kyoto-fu 611-0011, Japan

Received 22 August 2007; received in revised form 6 November 2007; accepted 12 November 2007
Available online 19 November 2007

Abstract

Phase separation and dewetting processes of blend thin films of polystyrene (PS) and poly(vinyl methyl ether) (PVME) in two phase region have been studied in a wide film thickness range from 65 μm to 42 nm ($\sim 2.5R_g$, R_g being radius of gyration of a polymer) using optical microscope (OM), atomic force microscope (AFM) and small-angle light scattering (LS). It was found that both phase separation and dewetting processes depend on the film thickness and were classified into four thickness regions. In the first region above $\sim$15 μm the spinodal decomposition (SD) type phase separation occurs in a similar manner to bulk and no dewetting is observed. This region can be regarded as bulk. In the second region between $\sim$15 and $\sim$1 μm, the SD type phase separation proceeds in the early stage while the characteristic wavelength of the SD decreases with the film thickness. In the late stage dewetting is induced by the phase separation. In the third region between $\sim$1 μm and $\sim$200 nm the dewetting is observed even in the early stage. The dewetting morphology is very irregular and no definite characteristic wavelength is observed. It is expected that the irregular morphology is induced by mixing up the characteristic wavelengths of the phase separation and the dewetting. In the fourth region below $\sim$200 nm the dewetting occurs after a long incubation time with a characteristic wavelength, which decreases with the film thickness. It is considered that the layered structure is formed in the thin film during the incubation period and triggers the dewetting through the capillary fluctuation mechanism or the composition fluctuation one.

Keywords: Polymer blend thin film; Phase separation; Dewetting

1. Introduction

Properties of polymer thin films on solid substrates are of great importance from scientific as well as industrial viewpoints because many important phenomena are related to the surface properties such as coating, adhesive, surface friction, lubricants, and dielectric layer [1–4]. Many studies on single component thin films have been carried out to reveal interesting but unusual properties of thin films. It was reported by many groups [5–9] that the glass transition temperature T_g decreased with film thickness below about 40 nm, and the thermal expansivity of the thin films is also a big issue under debate in the thin film research field [8–13]. Recently, dewetting and phase separation of polymer blend thin films are also of great interest because of technological applications as well as fundamental investigations. The dewetting of the phase separated polymer blend thin film limits the industrial applications because they require a stable, homogeneous and uniform thin films. This motivated the fundamental studies of polymer blend thin films very much to reveal the dewetting mechanism and control the morphology [4]. Stamm et al. [14] have extensively investigated blend thin films of poly(*p*-methylstyrene) (PpMS) and deuterated polystyrene (dPS), which was a weakly incompatible system, to find that the bilayer structure is formed via phase separation and the upper layer of poly(*p*-methylstyrene) dewetted on the lower layer of deuterated polystyrene. The blend thin films of poly(styrene-*ran*-acrylonitrile) (SAN) and deuterated poly(methyl methacrylate) (dPMMA) were also studied by some groups [15–20]. Chung and Composto recently examined the kinetics of phase separation in the blend thin films displaying discrete and bicontinuous domain morphologies [15], and found breakdown of dynamic scaling in the bicontinuous domain growth due to suppression of

* Corresponding author. Tel.: +81 774 38 3140; fax: +81 774 38 3146.
E-mail address: kanaya@scl.kyoto-u.ac.jp (T. Kanaya).

0032-3861/$ - see front matter © 2007 Elsevier Ltd. All rights reserved.
doi:10.1016/j.polymer.2007.11.031

lateral hydrodynamic pumping with decreasing film thickness while the scaling was hold in the discrete case. The same group also studied the dewetting mechanism of thin blend films of SAN and dPMMA in a wide thickness range [16–18] and presented a morphology map [19] based on the pattern development mechanism for thickness values and bulk composition between 50 and 1000 nm and $\varphi_{PMMA} = 0.3–0.8$, respectively. Recent works by Liao et al. [20] have experimentally demonstrated the dewetting mechanism induced by composition fluctuations [21–24] for thermodynamically stable ultrathin blend films of SAN and dPMMA in one phase region. In the two phase region dewetting of the whole film is followed by the phase separation in the droplets.

As for thin films of polystyrene (PS) and poly(vinyl methyl ether) (PVME) blend, which has a lower critical solution temperature (LCST) type phase diagram in bulk, Tanaka et al. [25] studied the surface structure of PS/PVME ultrathin films using atomic force microscopy (AFM) and observed dewetted droplets in one phase region for films thinner than twice the radius of gyration. Karim et al. [26,27] also reported similar undulation of the free surface in the two phase region where dPS is encapsulated by PVME in the thin film. These observations suggest that phase separation and dewetting competitively occur in ultrathin films of polymer blend. Small-angle light scattering studies on the kinetic of phase separation of PS/PVME blend thin films [28] show that the phase separation proceeds by a spinodal decomposition mechanism in a thick film (=180 nm) while in the thin film (=30 nm) it switches to nucleation and growth. However, there are no systematic studies on thin blend films of PS and PVME in a wide film thickness range.

In this study, therefore, we investigated morphology and kinetics of phase separation as well as dewetting in thin films of PS/PVME blends as a function of film thickness using light scattering (LS) techniques and optical microscope (OM) as well as using atomic force microscopy (AFM) in a wide thickness d range from semi-infinite thickness (65 μm) to that close to radius of gyration R_g of PS and PVME chains ($d \sim 2.5R_g$) to elucidate the relation between phase separation and dewetting in blend thin films of PS and PVME in the two phase region.

2. Experiment

Polystyrene (PS) and poly(vinyl methyl ether) (PVME) used in this study have weight-average molecular weights $M_w = 280{,}000$ and 90,000, and the molecular weight distributions in terms of $M_w/M_n = 3.01$ and 1.88, respectively, where M_n is number-average molecular weight. Both PS and PVME were purchased from Scientific Polymer Products, Inc. PS and PVME were purified by precipitating the toluene solutions into excess methanol and n-heptane several times, respectively, and dried in vacuum at room temperature for 72 h. It is noted that PS and PVME used in this experiment have similar values of radius of gyration R_g, which are 16.6 nm and 16.2 nm, respectively, although their molecular weights are different. Films below and above 1 μm were prepared by spin-coating and casting the toluene solution of PS and PVME, respectively, on a cleaned glass substrate after filtering with 2 μm pore size membrane at room temperature. The films were then annealed at 60 °C for 24 h after drying in vacuum at room temperature for 24 h. Thickness of polymer film was controlled by varying the polymer concentration in solution and confirmed with ellipsometer measurements.

Small-angle light scattering (LS) measurements were carried out using home-made apparatus with confocal collimation, which enables us to access a very low q range down to 0.1 μm^{-1} with extremely low background. These characteristic features enable us to measure such thin film as 42 nm. Two dimensional scattering intensities were accumulated every 5 min after temperature jump from one phase region to two phase region (=115 °C). Details of the LS instrument were reported elsewhere [29]. Optical microscope (OM) measurements were also done after temperature jump from one phase region to two phase region (=115 °C) using Olympus BX50 equipped with a CCD camera. Atomic force microscope (AFM) measurements were performed at room temperature after quenching the sample from two phase region (=115 °C) using JEOL JSPM-4200 to examine the surface morphology of the films.

3. Results and discussion

First of all we have constructed a phase diagram of the bulk PS/PVME blend. We observed LS intensity from samples with various blend ratios during the heating process from room temperature with a rate of 1 °C/min. It was reported [30] that the phase diagram does not depend on the heating rate when it is below 2 °C/min. In this measurement the cloud point was defined as an onset temperature of the scattering intensity. The phase diagram thus obtained is shown in Fig. 1, which is a lower critical solution temperature (LCST) type. The estimated critical weight fraction of PS φ_{PS} is 0.3 and the critical temperature T_c is 104.6 °C. At 115 °C the coexisting compositions are nearly pure components, which were estimated by extrapolating the phase diagram in Fig. 1. The glass transition temperature T_g of the bulk blend with the critical concentration ($\varphi_{PS} = 0.3$) is −20 °C. The phase

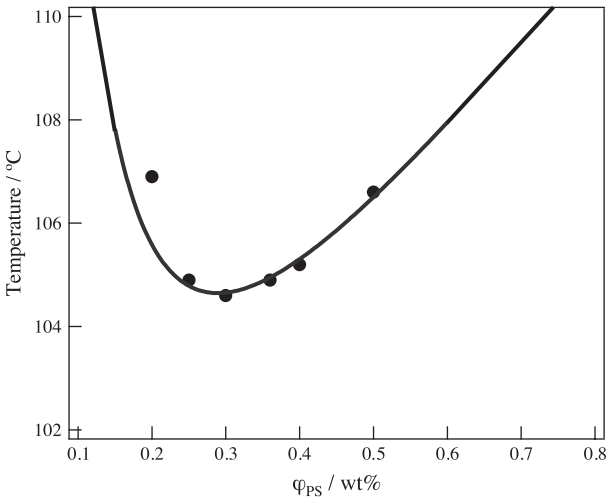

Fig. 1. Phase diagram of PS/PVME blend in bulk.

diagram is almost identical to the reported one [31]. In this work all LS, OM and AFM measurements were performed on PS/PVME blend thin films with the critical concentration of $\varphi_{PS} = 0.3$.

OM measurements were performed on the blend thin films as a function of annealing time after temperature jump to 115 °C in two phase region from one phase region. In addition the surface morphology was examined by AFM with contact mode after quenching the film to room temperature after 90 min annealing at 115 °C. The OM images are shown in Fig. 2 for 65 μm, 9 μm, 2 μm, 466 nm, 98 nm and 42 nm films at 20, 50, 90 and 120 min after the temperature jump, and the AFM results are given in Fig. 3. In the following we will discuss the OM and AFM results in order of the film thickness.

In the case of 65 μm film, the observed OM patterns look like typical SD phase separation process although they are 2D images, and the AFM results show that the surface is very smooth. These observations suggest that the SD type phase separation proceeds inside the 65 μm film. For the 9 and 2 μm films similar SD patterns are observed at 20 min in the early stage although the characteristic wavelengths seem smaller than those in the 65 μm film. The surfaces of the 9 and 2 μm films are very smooth, at least at 20 min, which was confirmed by AFM measurements. As the phase separation proceeds, some semi-irregular spot-like patterns with strong (white) contrast are observed over the SD pattern at 90 and 120 min in the later stage. This is well recognized in the OM image at 120 min for the 2 μm film (Fig. 2(c)). The AFM result in Fig. 3(b) clearly shows that the white spots are holes on the surface, confirming that the semi-irregular pattern is due to dewetting.

In the 466 nm film, the observed OM images are so irregular even at 20 and 50 min and grow with annealing time keeping the irregularity as seen in Fig. 2(d). The surface morphology examined by AFM confirmed that the irregular pattern was due to irregular dewetting morphology. As the film thickness further decreases, the time evolution of the OM and AFM images very much changed for the 98 and 42 nm films. In the first 20 or 30 min the OM images are very homogeneous and the surfaces examined by AFM are very smooth, implying that nothing happens. After the long incubation period regular bicontinuous morphologies with strong contrast are observed in the OM images, and finally become isolated droplets at 120 min. The AFM images of the 98 nm after 90 min annealing at 115 °C in Fig. 3(d) clearly shows that the regular pattern is due to the dewetting. The observed OM and AFM results show that the phase separation as well as dewetting in the PS/PVME blend thin film depends very much on the film thickness.

Concerning the dewetting in the blend thin films, it is emphasized that dewetting in one component (PS or PVME) films does not occur in such thick films as examined here. For example, dewetting occurs in PS films below about 5–6 nm [32] while it depends on temperature and molecular weight more or less. In any case, such thick one component films as 470 nm do not show dewetting. We also studied the stability of the blend films in a range from 42 nm to 65 μm at 90 °C in one phase region and found that no dewetting was observed during annealing at 90 °C for 6 h even in the 42 nm film, showing that the blend films are stable in one phase region. The present results suggest that dewetting observed in the PS/PVME thin films is induced by the phase separation.

In the next step, we studied the phase separation and dewetting of the PS/PVME blend thin films using time-resolved LS just after temperature jump to 115 °C in two phase region from one phase region. Fig. 4(a)–(f) shows the time evolutions of one dimensional (1D) LS profiles for the 65 μm, 9 μm, 2 μm, 466 nm, 98 nm and 42 nm films, which were obtained by circular averaging the 2D scattering profiles. The scattering profiles and their time evolutions clearly depend on the film thickness as observed in the OM and AFM measurements. In the 65 μm film the scattering profile shows a peak and its position gradually shifts to lower q with annealing time, showing typical spinodal decomposition (SD) type phase separation kinetics. In a rather thin film such as 2 μm, however, the time evolution of the scattering profile is different. In an early stage before ~30 min the time evolution of the scattering profile is very similar to that in the 65 μm film, however, the growth in the peak intensity is slowed down and the intensity in a low q range below the peak grows in a late stage after ~60 min. This must be caused by the semi-irregular holes on the surface due to the dewetting as seen in OM images (see Fig. 2(b) and (c)).

As the film thickness further decreases, the scattering peak disappears for films below ~1 μm as seen for the 466 nm film in Fig. 4(d). This must correspond to the irregular dewetting morphology observed in the OM and AFM measurements (see Figs. 2(d) and 3(c)). The scattering pattern obtained by fast Fourier transform (FFT) of the OM image of the 466 nm film does not show any peaks in the low q range down to 0.04 μm^{-1}, confirming that there are no characteristic wavelengths in the spatial scale below ~150 μm. With further decreasing the film thickness, surprisingly, the peak appears again below ~200 nm and the incubation time before the appearance of the peak is very long.

For quantitative discussions we plotted the peak intensity I_{max} and the peak position q_{max} as a function of annealing time in Fig. 5(a) and (b), respectively, for the 65 μm, 14 μm, 9 μm, 2 μm, 98 nm and 42 nm films. We first examined the results of the 65 μm film. The scattering peak appears at around 2 μm^{-1} at ~7 min after the temperature jump and the scattering intensity exponentially increases with annealing time before ~7 min. After ~7 min, as can be seen in Fig. 5(a) and (b), the peak intensity I_{max} and the peak position q_{max} increase according to power laws $I_{max}(t) \sim t^{\beta}$ and $q_{max}(t) \sim t^{-\alpha}$, respectively, suggesting that the scaling relations are hold. At around 30 min the slopes in $q_{max}(t) \sim t^{-\alpha}$ and $I_{max}(t) \sim t^{\beta}$ become steeper. The exponents α and β evaluated from the observed time evolutions of I_{max} and q_{max} are $\alpha = 0.25$ and $\beta = 0.85$ before 30 min and $\alpha = 0.54$ and $\beta = 1.62$ after 30 min, respectively, for the 65 μm film. These values are very close to those reported for the PS/PVME bulk blend by Hashimoto et al. [33,34], and the relations $\beta > 3\alpha$ and $\beta = 3\alpha$ are held before and after 30 min, respectively.

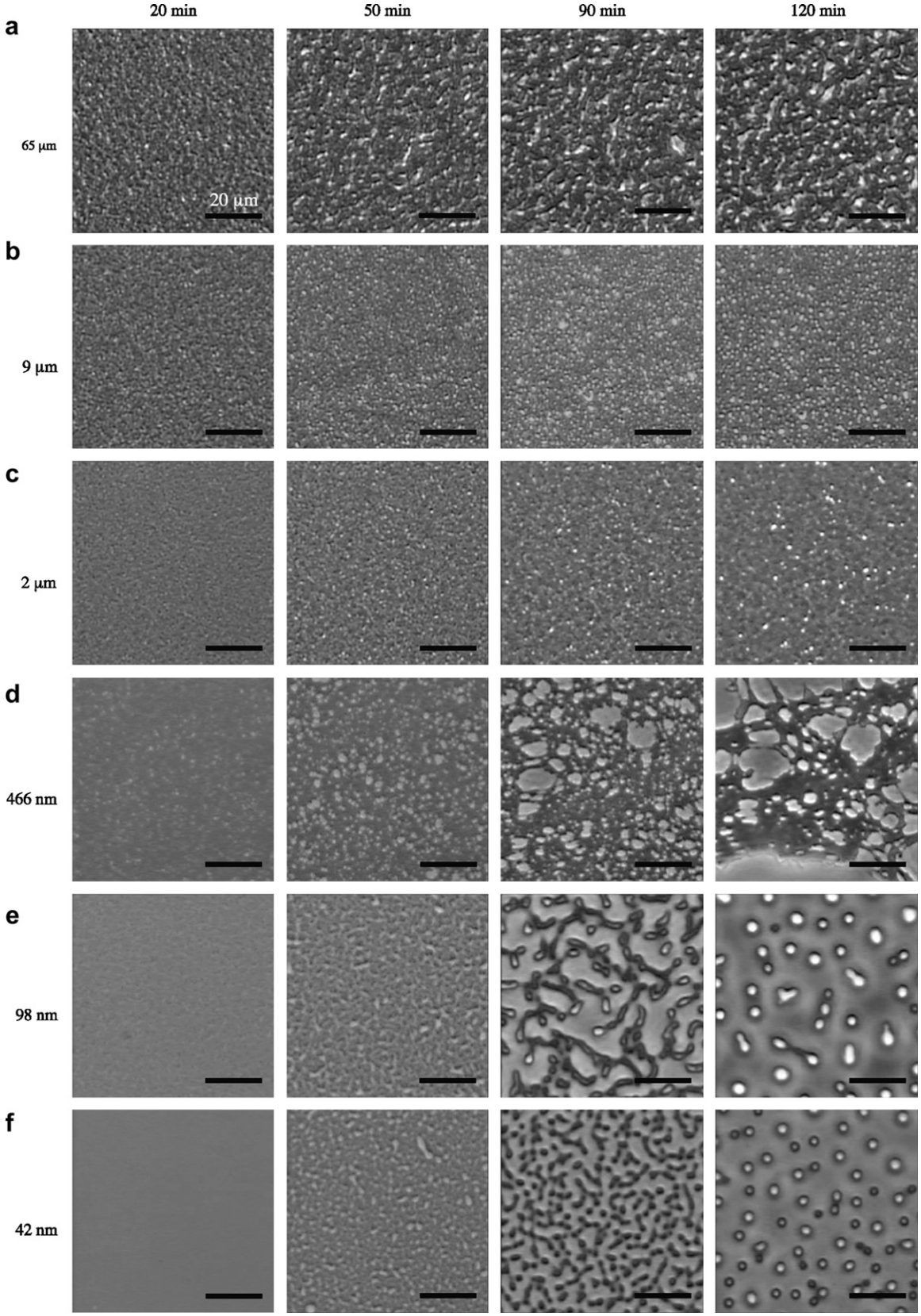

Fig. 2. Time evolution of OM images after temperature jump to 115 °C in two phase region from one phase region for film thickness (a) 65 μm, (b) 9 μm, (c) 2 μm, (d) 466 nm, (e) 98 nm and (f) 42 nm. Scale bars in OM images are 20 μm.

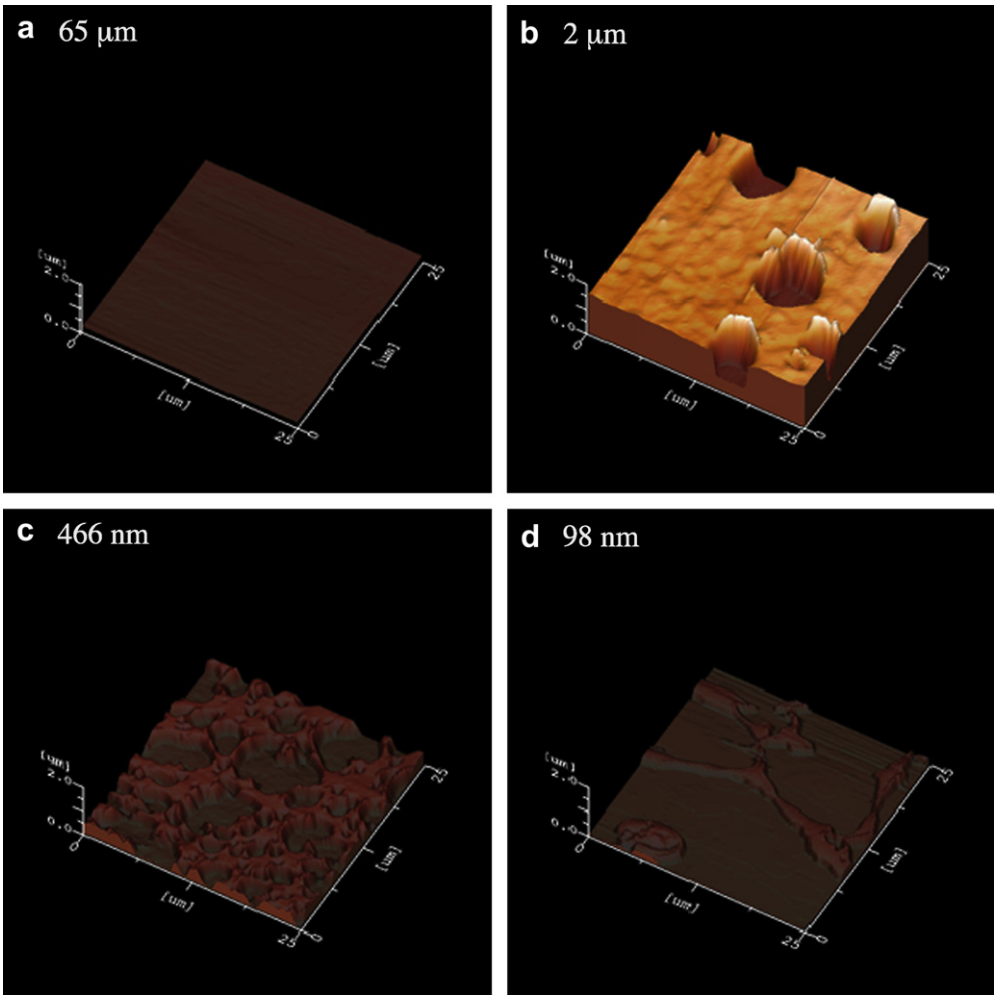

Fig. 3. AFM images of PS/PVME blend thin films quenched to room temperature after annealing at 115 °C in two phase region. (a) 65 μm after 90 min annealing, (b) 2 μm after 120 min annealing, (c) 466 nm after 90 min annealing and (d) 98 nm after 90 min annealing. *Z*-Range is 2.0 μm and *x*–*y* size is 25 μm × 25 μm for all images.

According to Hashimoto et al. the former and the latter can be regarded as the intermediate stage and the late stage of spinodal decomposition (SD) type phase separation, respectively [34]. From these LS results, we concluded that the 65 μm film could be regarded as a bulk sample. As mentioned above, we did not observe a scattering peak in the very early stage before ~7 min. This was also observed in the experiments by Hashimoto et al. [33,34].

The phase separation kinetics is almost independent of the film thickness for the films above ~15 μm. This region is termed Region I hereafter. On the other hand, as the film thickness decreases below ~15 μm, effects of the film thickness gradually appear on the kinetics. In the case of 14 μm film, the phase separation kinetics seems to be identical with that in the 65 μm film (bulk), at least, until ~20 min after the temperature jump as seen in Fig. 5. However, they deviate from the bulk behavior at ~20 min, showing some effects of film thickness. For films below ~15 μm and above ~1 μm, we observed similar level-off of the peak intensity after ~20 min. This region is termed Region II.

In order to see the differences between Region I and Region II, we plotted the characteristic wavelength λ_{max} ($=2\pi/q_{max}$) at 10 min after the temperature jump as a function of the film thickness in Fig. 6. In the figure the characteristic wavelength for the films below 200 nm is also plotted, which will be discussed later. The characteristic wavelength λ_{max} is almost constant for the films above ~15 μm (Region I), however, it begins to decrease with film thickness between ~15 and ~1 μm (Region II). When the characteristic wavelength λ_{max} encounters the film thickness d (thick solid line in Fig. 6) the characteristic peak disappears in the scattering profile, suggesting cut-off of the fluctuations with longer wavelength than the film thickness. In Fig. 7, the LS profiles at 10 min in the early stage after temperature jump are shown for the 2, 4 and 65 μm (bulk) films, the intensities of which were normalized to that at $q = 5\ \mu m^{-1}$ to compare the shapes of profiles. In the figure, q values corresponding to the film thickness ($q = 2\pi/d$) are indicated by down arrows. It is very clear that the scattering intensity in a q range lower than the scattering vector corresponding to the film thickness is suppressed, meaning that the fluctuations with wavelength longer than the film thickness are hard to appear in the thin films.

As the film thickness further decreases below ~1 μm, the scattering profiles are very different from those above

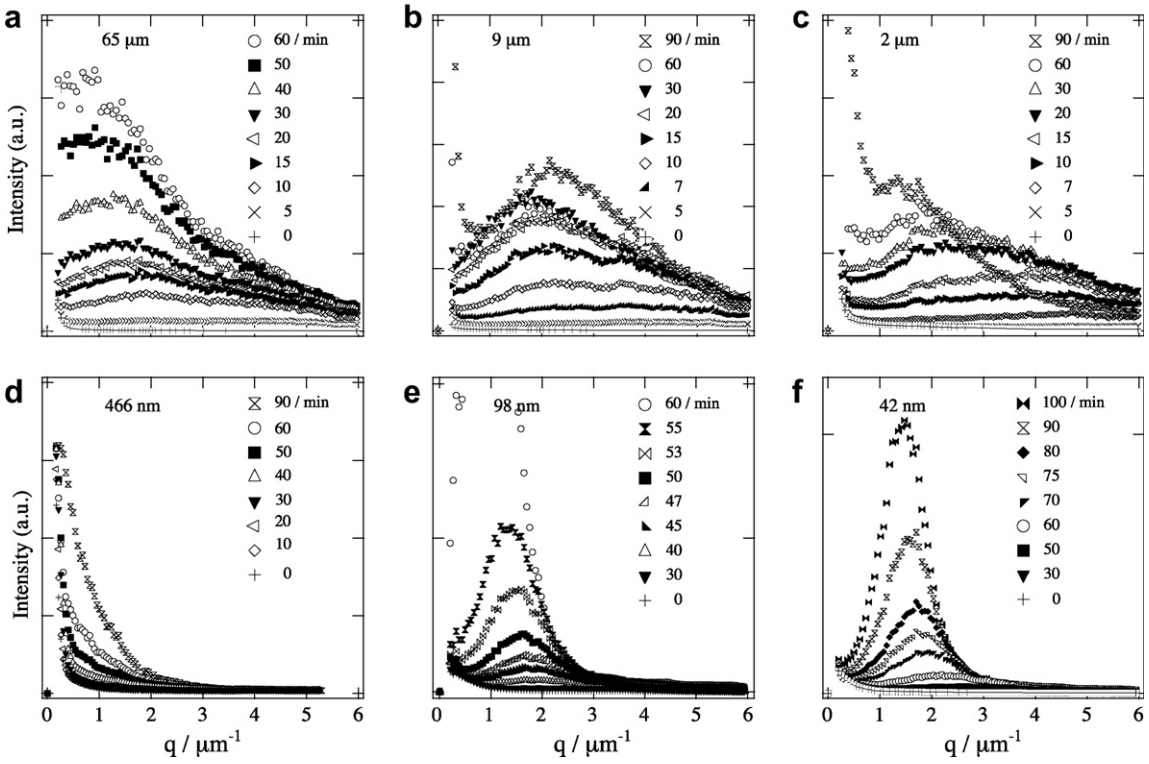

Fig. 4. Time evolution of LS profiles after temperature jump to 115 °C in two phase region from one phase region for film thickness (a) 65 μm, (b) 9 μm, (c) 2 μm, (d) 466 nm, (e) 98 nm and (f) 42 nm.

∼1 μm. As demonstrated for the 466 nm film (see Fig. 4(d)), no scattering peak is observed during the time evolution in the film thickness range between ∼1 μm and ∼200 nm, which is termed Region III. As shown in the OM and AFM measurements (Fig. 2(d) and Fig. 3(c)) this is due to the irregular dewetting morphology. However, at this moment we have no final conclusions on the irregular pattern. One possibility is that the phase separation and dewetting occur simultaneously and their characteristic wavelengths are mixed up, resulting in the irregular morphology.

For the films below ∼200 nm (Region IV) a scattering peak appears again (see Fig. 2). The time evolutions of the peak intensity I_{max} and the peak position q_{max} are shown for the 98 nm and 42 nm films in Fig. 5(a) and (b). This characteristic wavelength λ_{max} (=$2\pi/q_{max}$) is due to the dewetting as confirmed in the AFM measurements. The characteristic wavelength of dewetting in the early stage for the 98 nm film is larger than that of the SD phase separation in the films above ∼15 μm (Fig. 6), and decreases with the film thickness. This is one of the characteristic features of dewetting in the PS/PVME thin films below ∼200 nm (Region IV). Another characteristic feature is a very long incubation times before the appearance of the scattering peak, which are ∼30 min and ∼40 min for the 98 nm and 42 nm films, respectively.

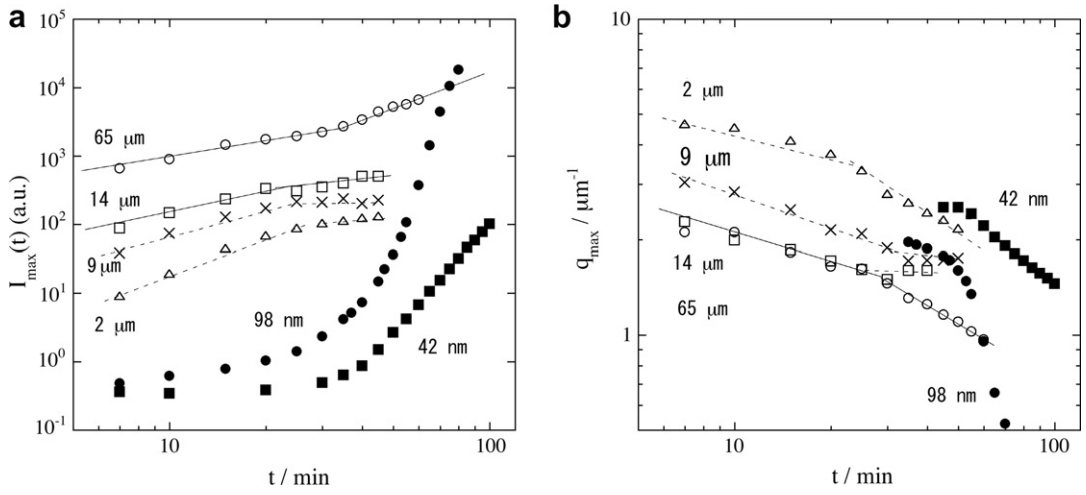

Fig. 5. Time evolution of (a) peak intensity I_{max} and (b) peak position q_{max} for film thickness 65 μm, 14 μm, 9 μm, 2 μm, 98 nm and 42 nm.

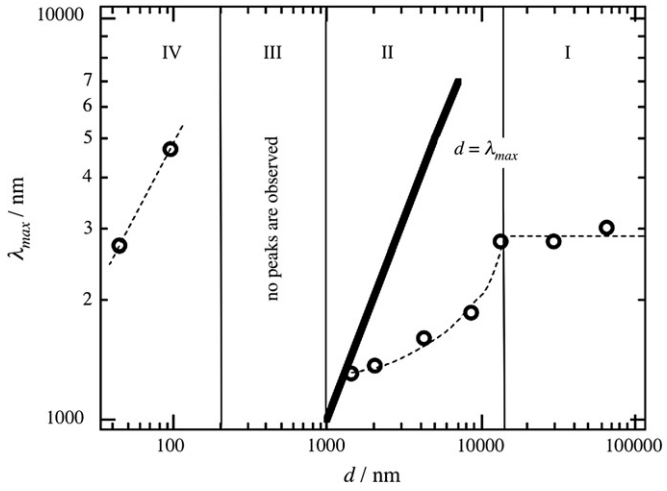

Fig. 6. Characteristic wavelength λ_{max} at 10 min (for Regions I and II) and at 50 min (for Region IV) after temperature jump to 115 °C in two phase region from one phase region as a function of film thickness. In Regions I and II, a thick solid line shows a relation that film thickness d is equal to characteristic wavelength λ_{max} ($d = \lambda_{max}$).

During the incubation period the scattering intensities hardly grow, while they increase very rapidly after the incubation period (see Fig. 5(b)) according to a power law with unexpected large exponents. In the following we will discuss the dewetting mechanisms in Regions II and IV.

In Region II, for example, we consider the 2 μm film. The scattering peak was observed at around $q_{max} = 5\ \mu m^{-1}$ in the early stage of phase separation and gradually shifted to lower q with annealing time (Fig. 5(b)). When q_{max} comes close to the film thickness ($q = 2\pi/2{-}3\ \mu m^{-1}$) at ~25 min, the growth of scattering intensity slows down or stops. Similar tendency was observed in the 9 and 14 μm films in Region II. From the OM results, it was also observed that the growth of phase

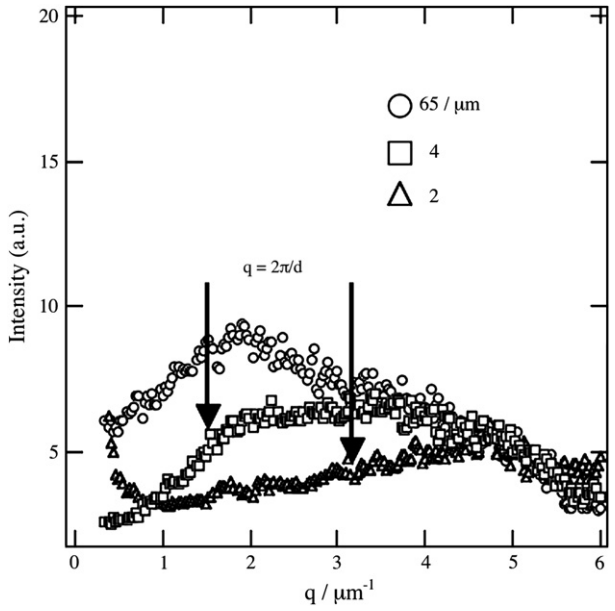

Fig. 7. LS profiles in the early stage of phase separation for the 65 μm, 4 μm and 2 μm films. The intensity is normalized to that at $q = 5\ \mu m^{-1}$.

separation stopped and the dewetting began to occur. These observations show that the composition fluctuations due to the SD phase separation induce the in-plane fluctuations on the surface/interface and rupture the film. An important problem we have to clarify is how the SD composition fluctuations induce the dewetting. Recently Chung et al. [35] have shown that phase separation drove dewetting in blend films of poly(methyl methacrylate) (PMMA) and poly(styrene-*ran*-acrylonitrile) (SAN) ($d = 550$ nm), and also shown that the capillary fluctuations failed to explain the roughening (or dewetting). On the basis of a universal scaling between the long wavelength fluctuations and surface roughness, they proposed that spinodal decomposition during initial phase separation may trigger the long wavelength fluctuations, and pointed out a possibility that the long wavelength fluctuations were created through the composition fluctuation mechanism proposed by Clarke [24]. In Region II, thus the dewetting induced by the SD composition fluctuations is one possible mechanism.

In Region IV, the regular patterns in the dewetting process suggest that the dewetting process proceeds through the SD mechanism. Generally speaking, however, SD type dewetting occurs when the system is in an unstable region and no incubation period is required [36,37]. The long incubation time means that some structure is formed before the dewetting in the thin film and the dewetting may be triggered by the structure. In the incubation period we see the very small increase in the LS intensity (see Fig. 5(a)) although it is not the SD type phase separation observed in Region II. This may suggest that some composition fluctuations proceed along the normal direction to the surface to form some layer structure, which are hard to be seen in the present scattering geometry with incident beam normal to the film surface. Such layer structure was reported for other polymer blend thin films. Stamm et al. [14] studied dewetting and phase separation in thin films of a weakly incompatible polymer blend of deuterated polystyrene (dPS) and poly(*p*-methylstyrene) (PpMS), and found that the interactions with substrate during the phase separation led to a bilayer formation with PpMS on the top layer. The bilayer structure is unstable and defines the starting point for the dewetting on the top of the dPS layer. In the final dewetting state a homogeneous layer of dPS on the top of the substrate is covered with ultrathin PpMS layer as well as the quite thick mesoscopic drops of PpMS. Apparently this mechanism is similar to our case. However, we observed bear Si surface in the AFM measurements, and hence no homogeneous layer of PVME was suggested. Blend thin films of deuterated poly(methyl methacrylate) (dPMMA) and poly(styrene-*ran*-acrylonitrile) (SAN) were also extensively studied by Composto et al. [15–18] in a wide thickness d range from semi-infinite limit to less than radius of gyration R_g of a polymer chain. In the semi-infinite limit they observed the so-called surface directed spinodal decomposition (SDSD), which is suppressed when the characteristic length is below the film thickness. In the thin film regions of $10R_g < d < 150R_g$ and of $\sim R_g < d < 10R_g$, tri-layer structure is formed in the early stage, consisting of surface and interface dPMMA-rich layers

and middle SAN-rich layer. In the SAN-rich middle layer they observed phase separated structure and homogeneous structure for the former and the latter, respectively. These reported results tell us that layered structure is easily formed due to the interactions between one of the blend component polymer and substrate (and/or air), and triggered the dewetting. We therefore expect tri-layer structure formation due to the preferential interactions between PVME and substrate at the interface and between PVME and air at the surface [38] before dewetting and the preliminary result of neutron reflectivity (NR) measurements on the deuterated PS/PVME blend thin films supported the tri-layer structure [39]. Note that the surface and interface segregation of PVME reduces the concentration of PVME in the middle bulk-like layer, but the preliminary NR results suggest that it is negligible for the films above ~50 nm [39].

For dewetting, the thin film must be ruptured by some mechanism. It was reported for dPMMA/SAN blend thin films ($10R_g < d < 150R_g$) [18] that the lateral phase coarsening occurs in the middle stage after the tri-layer structure formation, and finally the capillary fluctuations cause the thickness to vary and rapture the middle layer. Assuming the tri-layer structure formation in the PS/PVME blend thin film below ~200 nm (~$13R_g$) before dewetting, the situation is very similar to the dPMMA/SAN blend thin film. According to Wang and Composto [17] the characteristic wavelength of the capillary fluctuations Λ_m is given by

$$\Lambda_m = h_0^2[4\pi(\gamma_1 + \gamma_{12})/A]^{1/2} \quad (1)$$

for tri-layer structure. Here, h_0 is the initial thickness of the middle layer, γ_1 and γ_{12} are the surface and interfacial tensions of the top layer, and A is the Hamaker constant. Eq. (1) predicts that the characteristic wavelength of the dewetting decreases with the film thickness. This agrees with our observation shown in Fig. 5 although the detailed comparison is not impossible at the moment.

Recently An and co-workers [20] have explained the dewetting of thermodynamically stable blend ultrathin film of PMMA and SAN ($d \sim R_g$) in terms of a dewetting mechanism induced by composition fluctuations [20–23], which is a similar mechanism proposed in Region II. This mechanism may be possible even in two phase region. PVME has attractive interactions with Si substrate and air [38], and hence would diffuse to the substrate so as to create the composition gradient across the film. The diffusion could not occur homogeneously over the film surface to create the composition fluctuations in the mixture along the surface. When the amplitude of the fluctuations is large enough, the free surface is eventually destabilized, leading to the dewetting. At the moment we have no direct evidence for the dewetting mechanism in Region IV, but cannot deny both of them as a rapture mechanism for blend thin film. Investigation in the composition fluctuations normal to the surface would give us significant information on the dewetting mechanism.

4. Conclusion

In this study we investigated the morphology and the kinetics of phase separation and dewetting in blend thin films of PS/PVME as a function of film thickness from 42 nm to 65 μm using OM, AFM and LS. The time evolutions of OM images and LS patterns after the temperature jump into the two phase region strongly depend on the film thickness, and could be classified into four regions (Regions I, II, III and IV). In Region I above ~15 μm, the phase separation kinetics can be explained as normal SD phase separation in bulk. As the film thickness decreases, the characteristic wavelength to the SD phase separation becomes smaller with the film thickness in Region II between ~15 and ~1 μm because the composition fluctuations are suppressed by the film thickness. In Region II the films finally dewet in a very late stage, depending on the film thickness, which must be induced by the phase separation. In Region IV below ~200 nm the films dewet after a long incubation time. The bicontinuous morphologies with characteristic wavelength λ_{max} implies that the dewetting mechanism is a SD type, and the long incubation time was assigned to tri-layer structure formation. In Region III (1 μm–200 nm) between Region II and Region IV the LS patterns do not show any characteristic scattering peaks, corresponding to the irregular dewetting pattern confirmed by AFM. It suggests that the phase separation and dewetting occur simultaneously and their characteristic wavelengths are mixed up, resulting in the irregular morphology. In Regions II and IV the dewetting mechanisms were discussed. In Region II the dewetting induced by the SD composition fluctuations was proposed. In Region IV below ~200 nm preferential interactions between one component of blend polymers (PVME) and substrate as well as air lead to vertical phase separation to create tri-layer structure, consisting of interface and surface PVME layers and the middle blend layer. For dewetting, the middle layer must be ruptured by some mechanism. One possibility is the capillary fluctuations and the other is the composition fluctuations at the interlayer. This will be confirmed in near future by neutron reflectivity measurements.

References

[1] Jones RL, Richards RW. Polymers at surface and interfaces. Cambridge: Cambridge University Press; 1999.
[2] Karim A, Kumar S. Polymer surfaces, interfaces and thin films. Singapore: World Scientific; 2000.
[3] Bucknall DG. Prog Mater Sci 2004;49:713–86.
[4] Mueller-Buschbaum P, Bauer E, Wunnicke O, Stamm M. J Phys Condens Matter 2005;17:S363–86.
[5] Keddie JL, Jones RA, Cory RA. Europhys Lett. 1994;27:59–64.
[6] Keddie JL, Jones RA, Cory RA. Faraday Discuss 1994;98:219–30.
[7] Forrest JA, Dalnoki-Veress K, Stevens JR, Dutcher JR. Phys Rev Lett 1996;77:2002–5.
[8] Kawana S, Jones RAL. Phys Rev E 2001;63:021501-1–6.
[9] Miyazaki T, Nishida K, Kanaya T. Phys Rev E 2004;69:06183–8.
[10] Orts WJ, Zanten JHv, Wu W, Satija SK. Phys Rev Lett 1993;71:867–70.
[11] Fukao K, Miyamoto Y. Phys Rev E 2000;61:1743–54.
[12] DeMaggio GB, Frieze WE, Gidley DW, Zhu M, Hristov HA, Yee AF. Phys Rev Lett 1997;78:1524–7.

[13] Kanaya T, Miyazaki T, Watanabe H, Nishida K, Yamano H, Tasaki S, et al. Polymer 2003;44:3769–73.
[14] Mueller-Buschbaum P, O'Neil SA, Affrossman S, Stamm M. Macromolecules 1998;31:5003–9.
[15] Chung H, Composto RJ. Phys Rev Lett 2004;92:185704–7.
[16] Wang H, Composto RJ. Europhys Lett 2000;50:622–7.
[17] Wang H, Composto RJ. J Chem Phys 2000;113:10386–97.
[18] Wang H, Composto RJ. Interface Sci 2003;11:237–48.
[19] Chung H-j, Wang H, Composto RJ. Macromolecules 2006;39:153–61.
[20] Liao Y, Su Z, Sun Z, Shi T, An L. Macromol Rapid Commun 2006;27:351–5.
[21] Wensink KDF, Je'remoe B. Langmuir 2002;18:413–6.
[22] Sharma A, Mittal J. Phys Rev Lett 2002;89:186101–4.
[23] Sharma A, MIttal J, Verma R. Langmuir 2002;18:10213–20.
[24] Clarke N. Macromolecules 2005;38:6775–8.
[25] Tanaka K, Yoon JS, Takahara A, Kajiyama T. Macromolecules 1995; 28:934–8.
[26] Ermi BD, Karim A, Douglas JF. J Polym Sci Part B 1998;36: 191–200.
[27] Karim A, Slawecki TM, Kumar SK, Douglas JF, Satija SK, Han CC, et al. Macromolecules 1998:857–62.
[28] El-Mabrouk K, Belaiche M, Bousmina M. J Colloid Interface Sci 2007; 306:354–67.
[29] Nishida K, Kanaya T, Matsuba G, Ogawa H, Konishi T. Japanese Patent Pending 2005-058211; 2005.
[30] El-Mabrouk K, Bousmina M. Rheol Acta 2006;45:877–89.
[31] Hashimoto T, Itakura M, Hasegawa H. J Chem Phys 1986;85:6118–28.
[32] Reiter G. Macromolecules 1994;27:3046–52.
[33] Hashimoto T, Kumaki J, Kawai H. Macromolecules 1983;16:641–8.
[34] Hashimoto T, Itakura M, Shimidzu N. J Chem Phys 1986;85:6773–86.
[35] Chung H-j, Ohno K, Fukuda T, Composto RJ. Macromolecules 2007; 40:384–8.
[36] Cahn JW, Hilliard JE. J Chem Phys 1958;28:258–67.
[37] Cahn JW. J Chem Phys 1965;42:93–9.
[38] Forrey C, Koberstein J, Pan DH. Interface Sci 2003;11:211–23.
[39] Kanaya T, Ogawa H, Nishida K, Matsuba G. Book of abstracts, Juelich Soft Matter Days, Bonn, Germany; 14–17 November, 2006.